ARL-TR-7482 ● SEP 2015

US Army Research Laboratory

Thermal Fluid Analysis of the Combustor Test Setup for a US Army Research Laboratory (ARL) Liquid-Fueled Thermophotovoltaic Power Source Demonstrator

by William R Allmon and Dr C Mike Waits

NOTICES

Disclaimers

The findings in this report are not to be construed as an official Department of the Army position unless so designated by other authorized documents.

Citation of manufacturer's or trade names does not constitute an official endorsement or approval of the use thereof.

Destroy this report when it is no longer needed. Do not return it to the originator.

ARL-TR-7482 ● SEP 2015

US Army Research Laboratory

Thermal Fluid Analysis of the Combustor Test Setup for a US Army Research Laboratory (ARL) Liquid-Fueled Thermophotovoltaic Power Source Demonstrator

by William R Allmon and Dr C Mike Waits
Sensors and Electron Devices Directorate, ARL

REPORT DOCUMENTATION PAGE

Form Approved
OMB No. 0704-0188

1. REPORT DATE *(DD-MM-YYYY)*	2. REPORT TYPE	3. DATES COVERED (From - To)
Sep 2015	Final	

4. TITLE AND SUBTITLE
Thermal Fluid Analysis of the Combustor Test Setup for a US Army Research Laboratory (ARL) Liquid-Fueled Thermophotovoltaic Power Source Demonstrator

5a. CONTRACT NUMBER

5b. GRANT NUMBER

5c. PROGRAM ELEMENT NUMBER

6. AUTHOR(S)
William R Allmon and Dr C Mike Waits

5d. PROJECT NUMBER

5e. TASK NUMBER

5f. WORK UNIT NUMBER

7. PERFORMING ORGANIZATION NAME(S) AND ADDRESS(ES)
US Army Research Laboratory
ATTN: RDRL-SED-E
2800 Powder Mill Road
Adelphi, MD 20783-1138

8. PERFORMING ORGANIZATION REPORT NUMBER
ARL-TR-7482

9. SPONSORING/MONITORING AGENCY NAME(S) AND ADDRESS(ES)

10. SPONSOR/MONITOR'S ACRONYM(S)

11. SPONSOR/MONITOR'S REPORT NUMBER(S)

12. DISTRIBUTION/AVAILABILITY STATEMENT
Approved for public release; distribution unlimited.

13. SUPPLEMENTARY NOTES

14. ABSTRACT

Compact power sources with high energy and power densities are critical for many military applications. These applications span from personal or squad-level power sources for long duration missions without resupply to unmanned air vehicles (UAVs) requiring only a few hours of running time. In the 10–100 W+ power range, battery technology is the best solution currently available, but higher energy dense technologies are needed to augment batteries and extend the available energy density well beyond state of the art battery technology. One way to approach this is to take advantage of the large energy content of hydrocarbons or alcohols. Conversion efficiencies of only a few percent can provide comparable energy density to battery technology with the added advantage of instant recharge. One technology being pursued by the US Army Research Laboratory (ARL) is combustion-based thermophotovoltaic (TPV) power sources. Combustion can be used to convert fuel to heat a surface to temperatures above 500 °C. A Combustor Test Setup is being developed to allow testing of various combustors in vacuum. The purpose of this report is to estimate the temperatures of various components of the Combustor Test Setup to ensure proper function.

15. SUBJECT TERMS
Power Source, Thermophotovoltaic (TPV), Combustion, Computational Fluid Dynamics (CFD), Thermal Fluid, Liquid Fuel

16. SECURITY CLASSIFICATION OF:			17. LIMITATION OF ABSTRACT	18. NUMBER OF PAGES	19a. NAME OF RESPONSIBLE PERSON
a. REPORT	b. ABSTRACT	c. THIS PAGE			William R Allmon
Unclassified	Unclassified	Unclassified	UU	34	19b. TELEPHONE NUMBER (Include area code) 301-394-0117

Contents

List of Figures

List of Tables

INTENTIONALLY LEFT BLANK.

1. Background

Compact power sources with high energy and power densities are critical for many military applications. These applications span from personal or squad-level power sources for long duration missions without resupply to unmanned air vehicles (UAVs) requiring only a few hours of running time. In the 10–100 W+ power range, battery technology is the best solution currently available. But higher energy dense technologies are needed to augment batteries and extend the available energy density well beyond state-of-the-art battery technology (140 W·h/kg for rechargeable lithium [Li]-ion technology).[1]

One way to approach this is to take advantage of the large energy content of hydrocarbons or alcohols. Conversion efficiencies of only a few percent can provide comparable energy density to battery technology with the added advantage of instant recharge. One technology being pursued by the US Army Research Laboratory (ARL) is combustion-based thermophotovoltaic (TPV) power sources including a microcombustor and heat recuperator. Combustion can be used to convert fuel to heat a surface to temperatures above 500 °C.[1]

Figure 1 describes the primary components of a TPV system: a heat source, an emitter, and a photovoltaic converter. The heat source supplies thermal energy to the emitter, which radiates the energy across a gap to the photovoltaic cell or an array of photovoltaic cells. The photovoltaic cell(s) then converts the thermal radiation to electrical energy, which can be delivered to a load or conditioning circuitry. Optical filters between the emitter and the photovoltaic cell (not included in Fig. 1), as well as the reflectors deposited on the backside of the photovoltaic cell, are also common components. The optical cavity between the emitter and photovoltaic cell is often held under vacuum to minimize conduction and convective heat transfer.[1] For the concept demonstrator being developed at ARL, the exterior of the heat recuperator and microcombustor will also be held at vacuum to minimize heat loss.

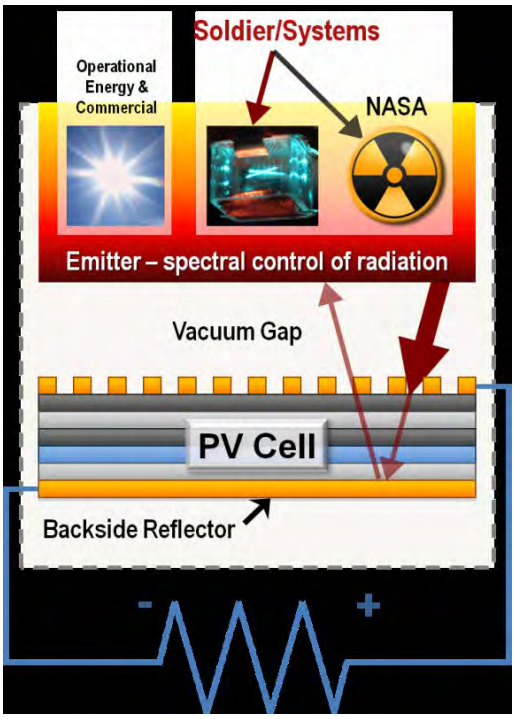

Fig. 1 Primary components of the TPV energy converter[1]

2. Introduction

To support the development of the concept demonstrator, a Combustor Test Setup is being developed. The Combustor Test Setup will allow testing of various combustors in vacuum. Figure 2 shows the combustor with the associated tubing and vacuum flange.

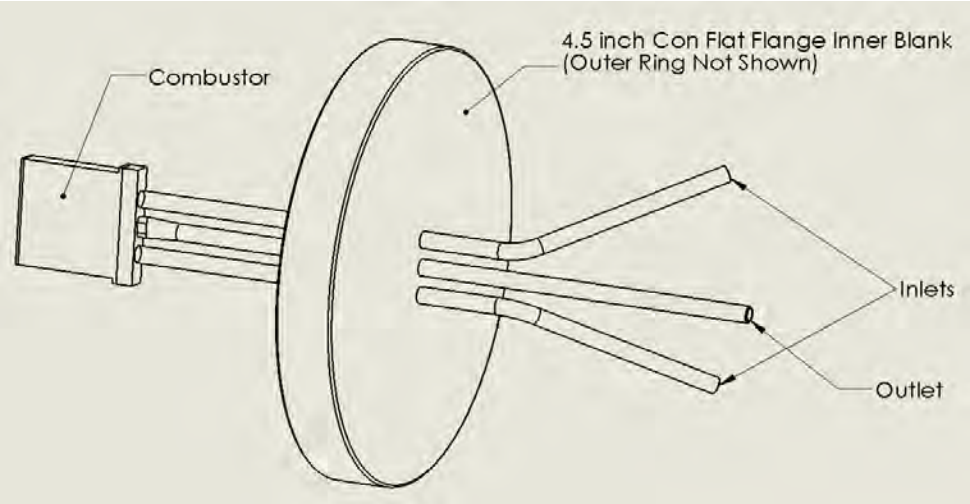

Fig. 2 Combustor with the associated tubing and vacuum flange

Figure 3 shows the cross sections of the combustor through an inlet and outlet tube. Note the design features recirculation where the flow passes through the outer passages of the combustor, reverses direction, and exhausts through the center passage of the combustor.

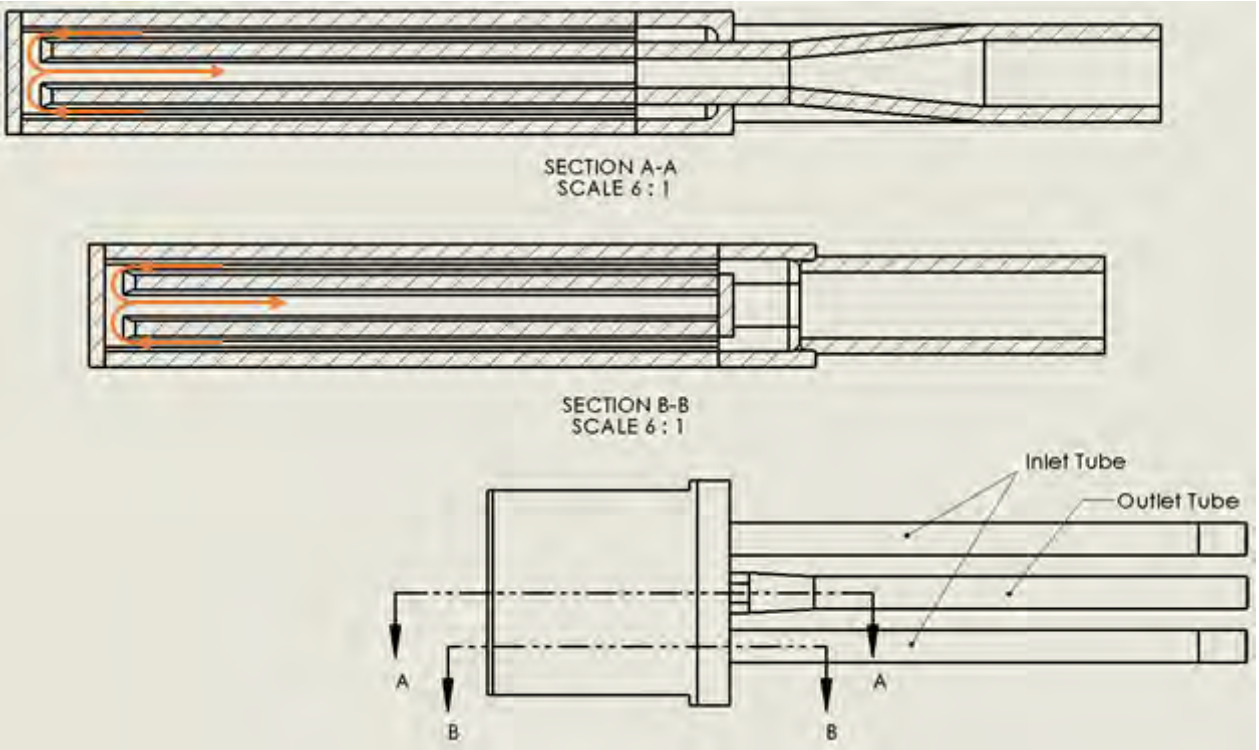

Fig. 3 Cross sections of the combustor

Figure 4 shows the entire Combustor Test Setup to include the vacuum chamber (cube), the turbo molecular drag pump connected to the vacuum chamber via a mitered elbow, gages, and associated vacuum components.

The purpose of this report is to estimate the temperatures of various components of the Combustor Test Setup to ensure proper function. Specific areas of concern include the temperature of the combustor, vacuum chamber wall near the tubes, tubes, exhaust gas, and flanges where the viewport and pump are to be attached. We want to ensure the predicted temperatures are within the operating temperature of the material or component selected. In addition, we want to know these temperatures for personnel safety.

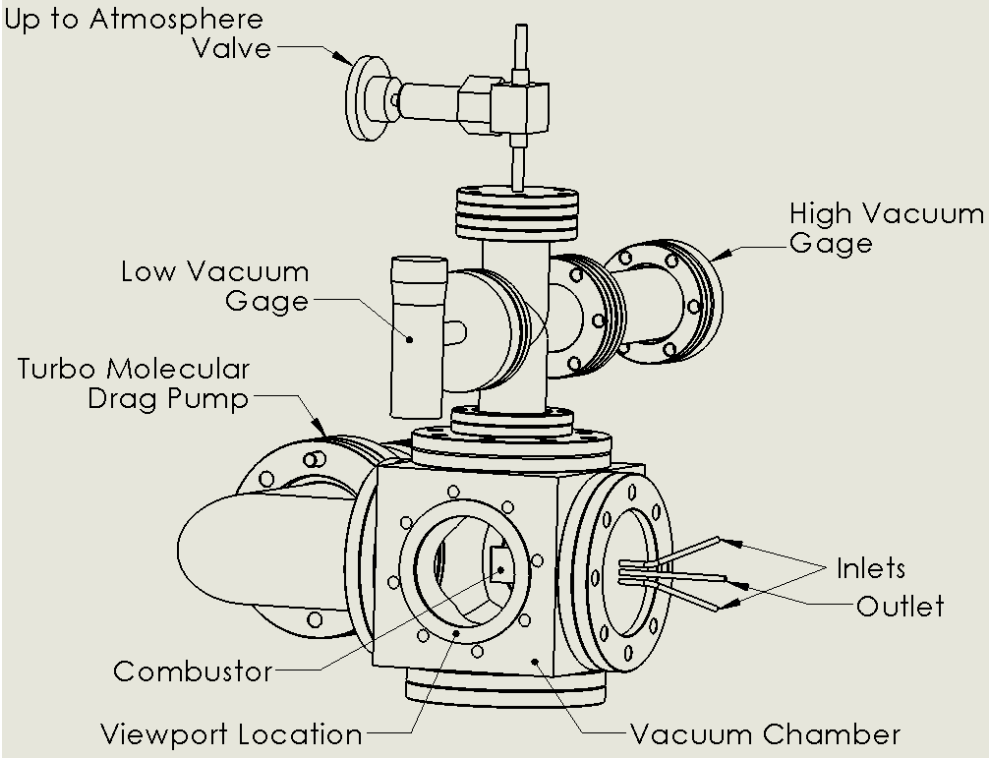

Fig. 4 Combustor Test Setup

3. Thermal Fluid Analysis

Thermal fluid analysis enables analysis of conjugate heat transfer (thermal conduction in solids, convection between fluids and solids, and radiation) using computational fluid dynamics (CFD) to detect hot spots, reduce overheating challenges, improve thermal isolation, and leverage thermal performance. This analysis was completed using Solid Works Flow Simulation, which can calculate either the steady-state or transient temperature fields due to heat transfer in solids (conduction); free, forced, and mixed convection; radiation; and heat sources (heat generation rate, heat power, temperature).[2]

4. Software Set Up

One of the first steps in the analysis process is to simplify the geometry. Figure 5 shows the simplified geometry used where the details of parts are eliminated to make the geometry easier to mesh and to eliminate discontinuities in the mesh.

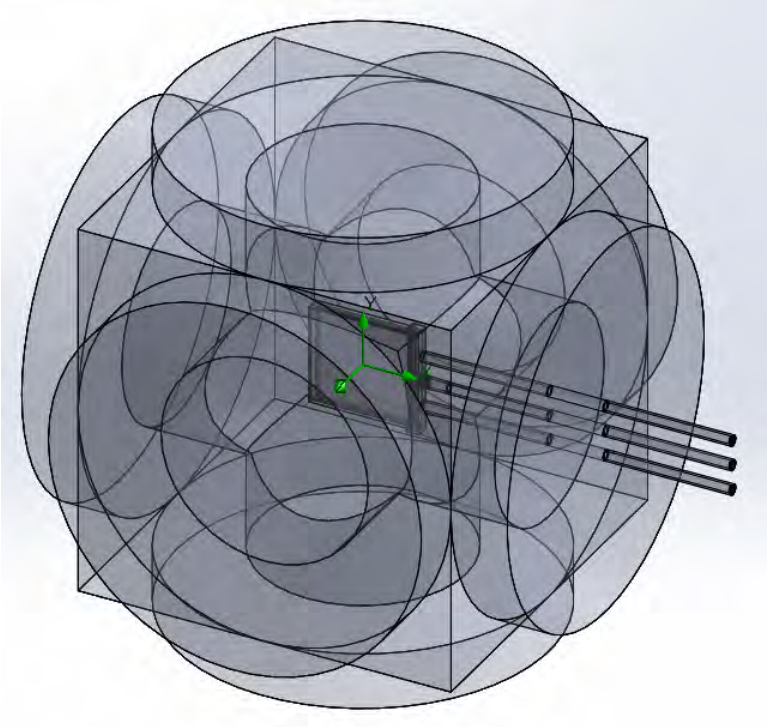

Fig. 5 Simplified geometry of the Combustor Test Setup

Heat conduction in solids, free and forced convection, and radiation are included in the analysis. For fluids, we simplify our fuel and air mixture to consider it as air only since the majority of the fluid is air. The flow conditions are considered as laminar and turbulent. For solids, user-defined solids, 304 Stainless Steel and Inconel 600, were added with the properties shown in Figs. 6–10.

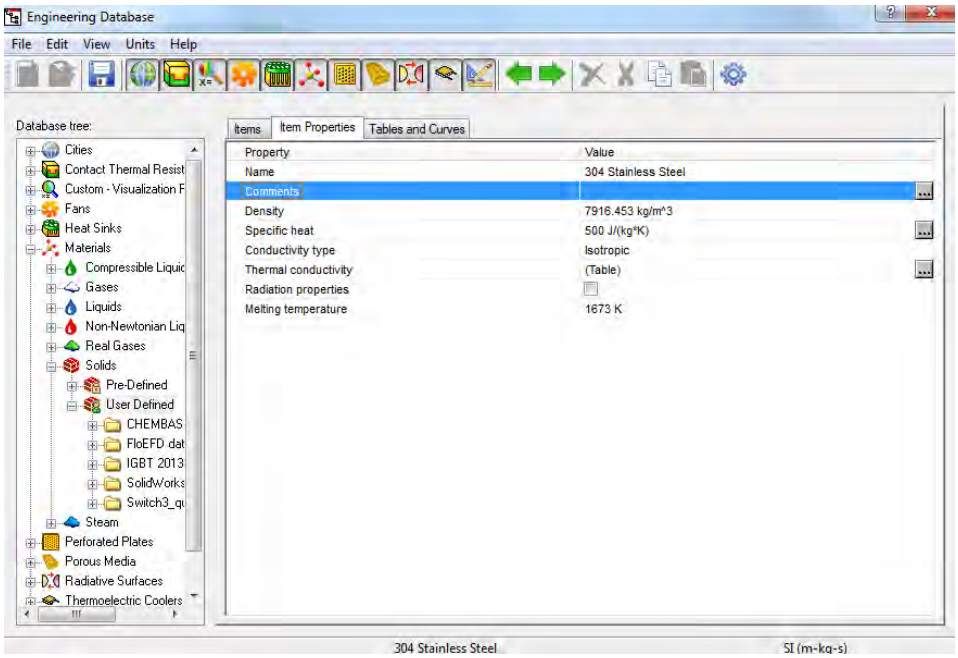

Fig. 6 Properties of the user-defined 304 Stainless Steel[3]

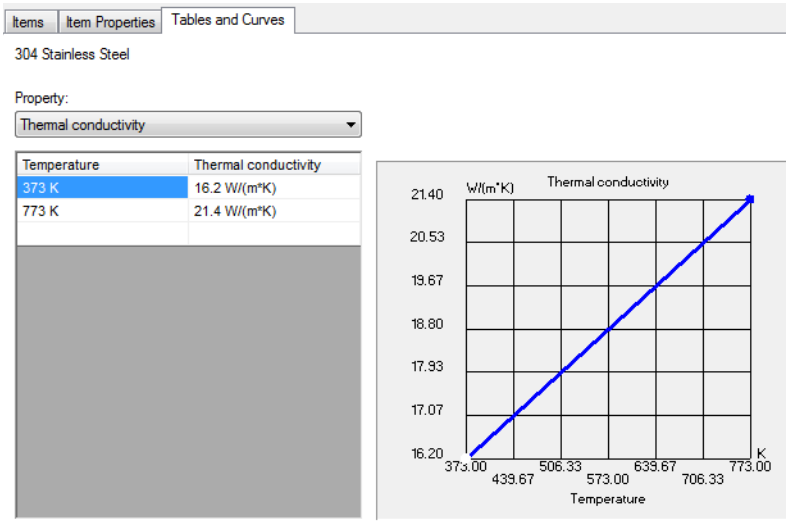

Fig. 7 Thermal conductivity vs. temperature for the user-defined 304 Stainless Steel[3]

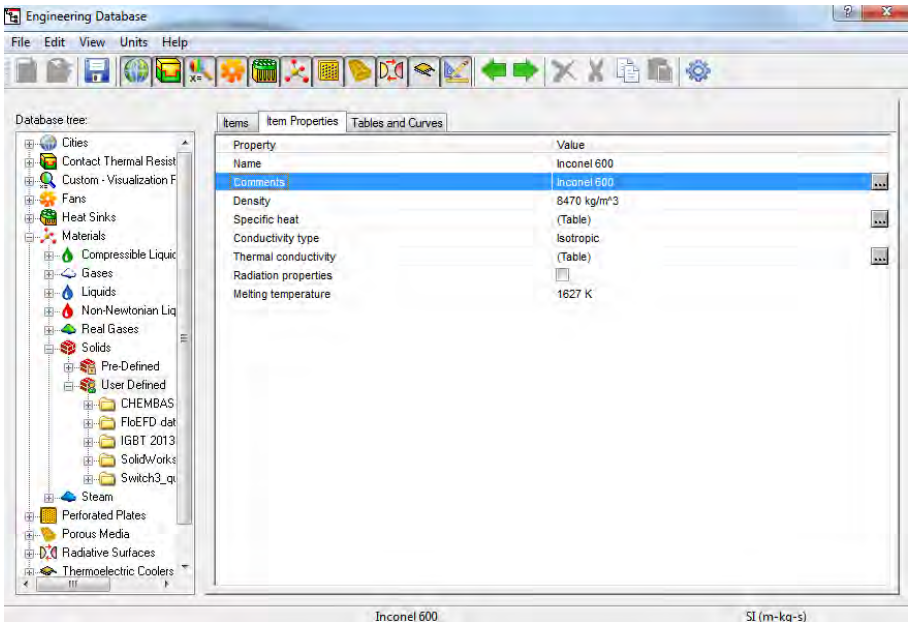

Fig. 8 Properties of the user-defined Inconel 600[4]

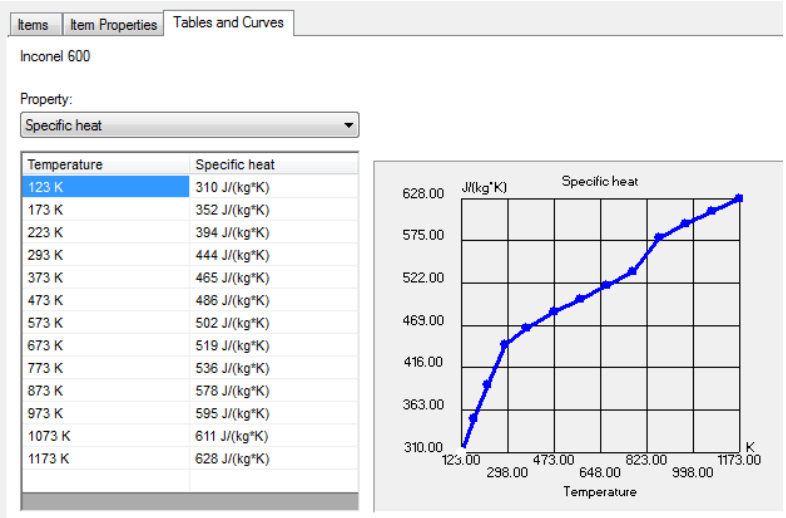

Fig. 9 Specific heat vs. temperature for the user-defined Inconel 600[4]

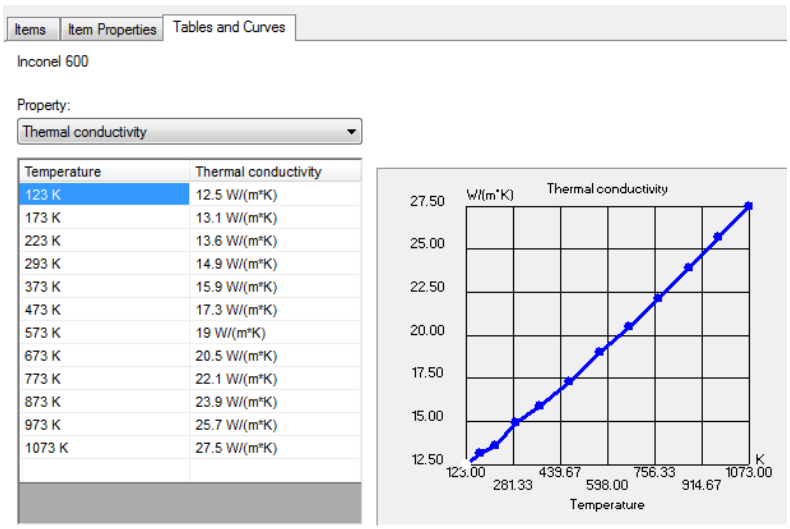

Fig. 10 Thermal conductivity vs. temperature for the user-defined Inconel 600[4]

For wall conditions, the outer wall thermal condition relied on the heat transfer coefficient of 20 W/m^{2}K, which is a typical value for free convection in air. The external air temperature was set to 20.05 °C. Since radiation at the estimate temperatures of the exterior of the system is small, the default was set to non-radiating. Later in this report, specific radiating surface properties are assigned to specific surfaces.

Based on work with other combustors, the worst-case heat generation rate was set to 300 W on the surface of the combustor and the flow rate of 0.105944 ft^3/min (3 L/min) for each inlet tube was used. The outlet tube cap was set to ambient pressure. Figure 11 shows where these values were applied.

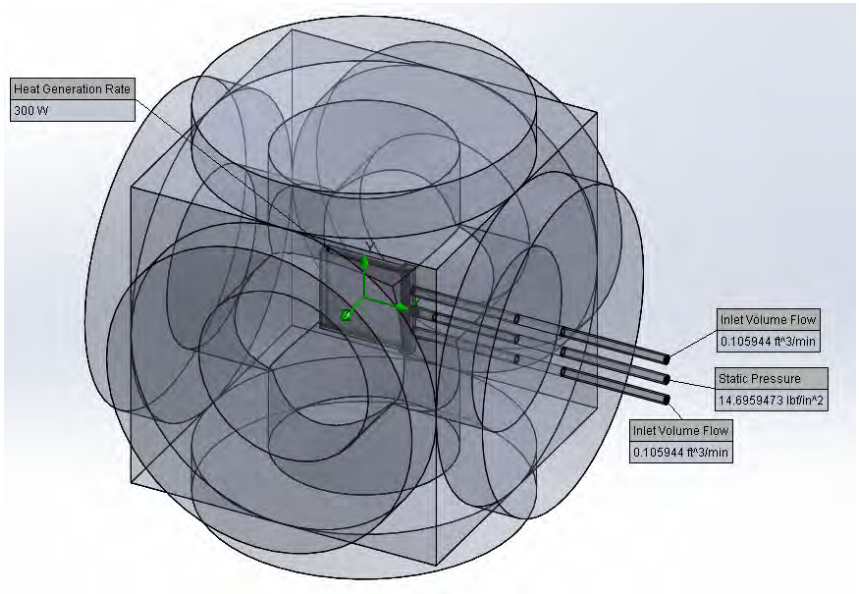

Fig. 11 Heat generation rate, inlet flows, and static outlet pressure

Figure 12 shows which components were assigned to the user-defined properties of 304 Stainless Steel.

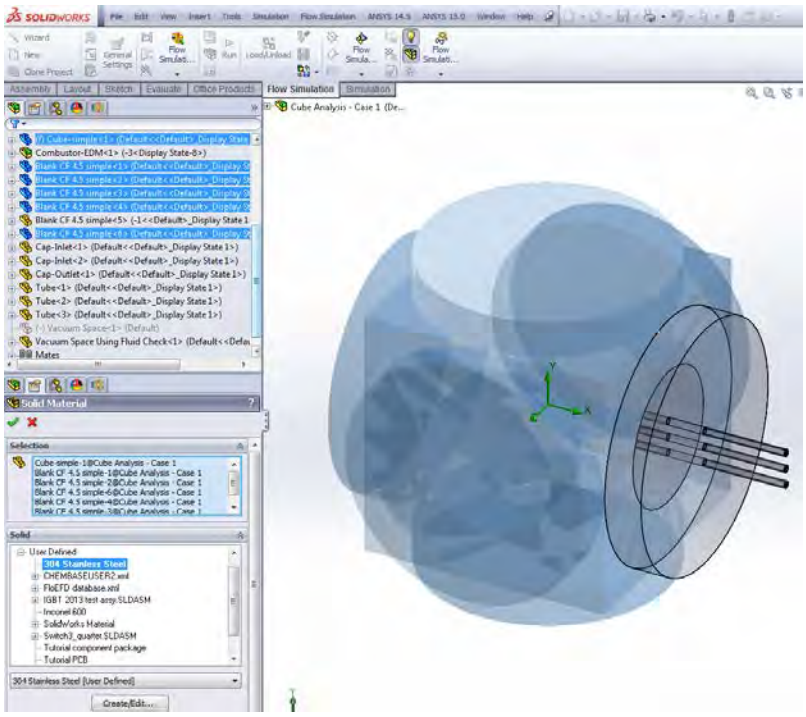

Fig. 12 Components assigned to the user-defined properties of 304 Stainless Steel

Figure 13 shows which components were assigned to the user-defined properties of Inconel 600.

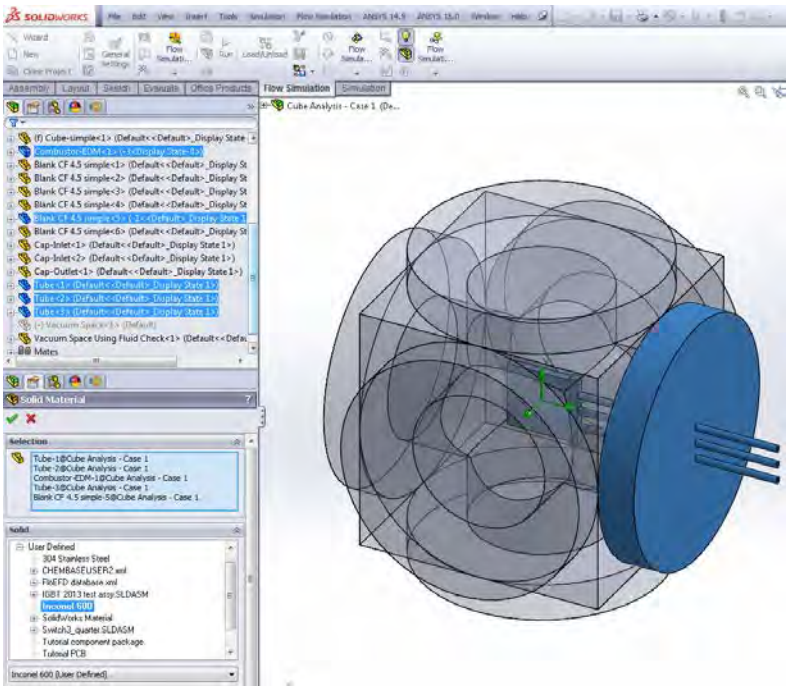

Fig. 13 Components assigned to the user-defined properties of Inconel 600

Figure 14 shows that the vacuum space was assigned to the properties of an insulator.

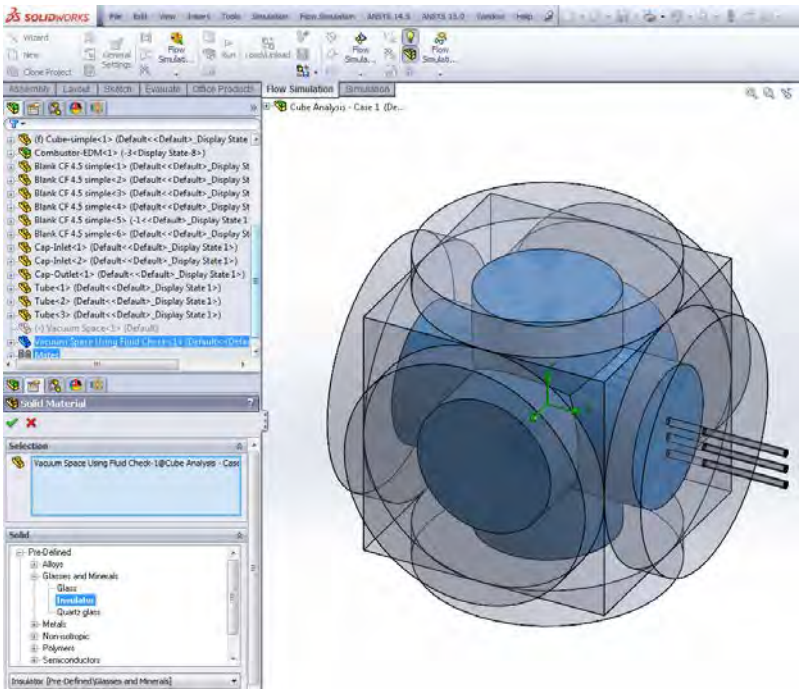

Fig. 14 Vacuum space

The insulator properties assigned to the vacuum space are shown in Fig. 15.

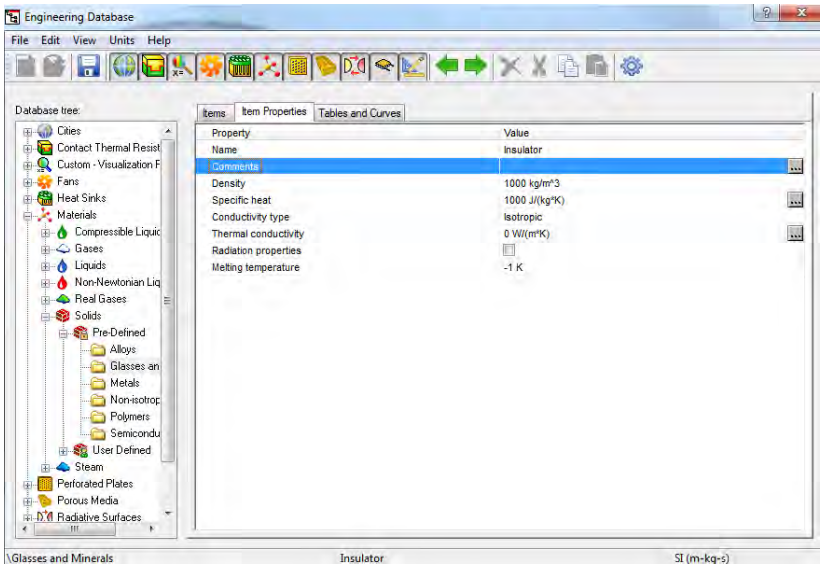

Fig. 15 Insulator properties

Figure 16 defines the radiative surface properties for 304 polished stainless steel. Vacuum components are mostly made of polished 304 stainless steel. The property

was named “304 Polished Stainless Steel–Allmon” and assigned to all the same 304 Stainless Steel components, as shown in Fig. 12.

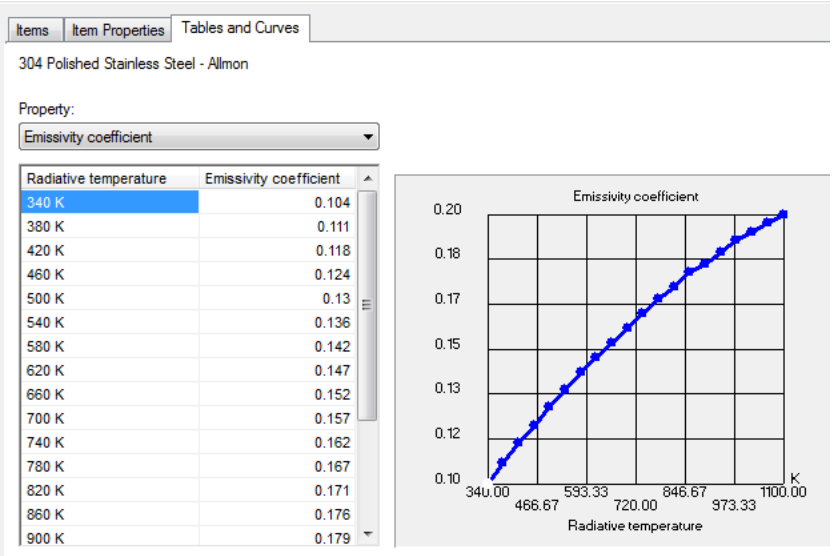

Fig. 16 Emissivity coefficient vs. temperature for 304 Polished Stainless Steel[5]

Radiative surface properties were defined for Inconel 600 and named “Inconel 600 radiation” (Fig. 17). This radiative surface property was assigned to all the components are the Inconel 600, as shown in Fig. 13.

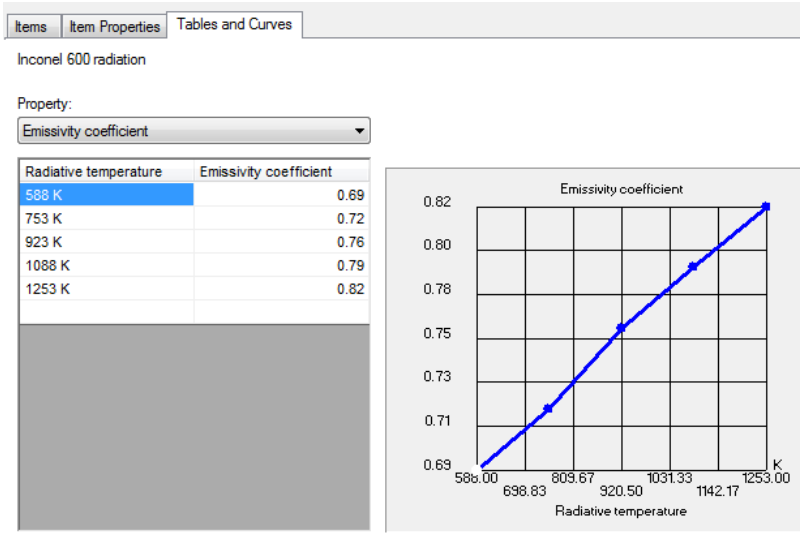

Fig. 17 Emissivity coefficient vs. temperature for Inconel 600[4]

5. Mesh

Two runs with the setup above were run successfully. For the first run, the initial mesh had the minimum gap size set to 0.04 inch and the level of the initial mesh

was set to 3. For the second run, the initial mesh had a minimum gap size of 0.01 inch and level of initial mesh was set to 5. Both runs had the option to optimize thin wall resolution checked. Figures 18 and 19 show the mesh in the area of the outlet tube and lower inlet tube where they pass through the vacuum chamber wall for Run 1 and 2, respectively. Note the coarser mesh of the tubes and around the hole in the vacuum chamber wall for Run 1 compared to Run 2.

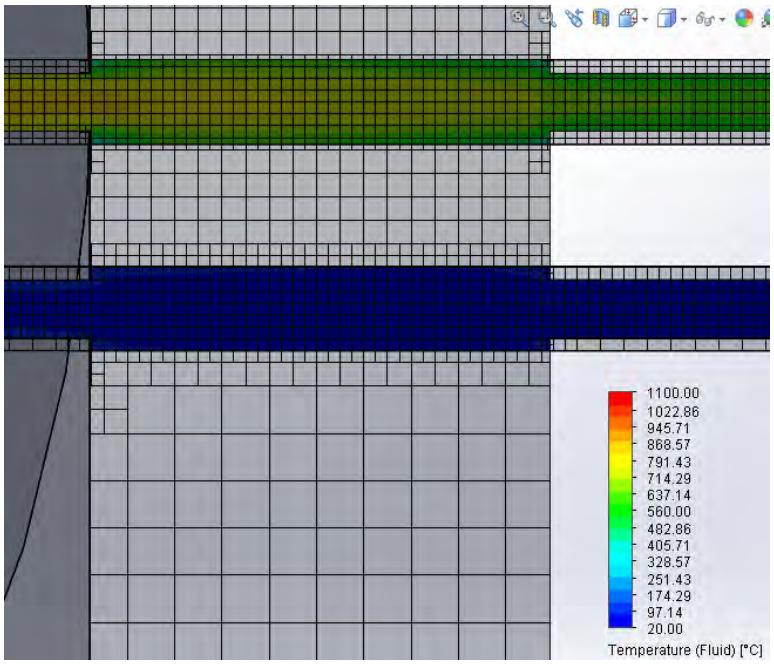

Fig. 18 Run 1 mesh in the area of the outlet tube and lower inlet tube where they pass through the vacuum chamber wall

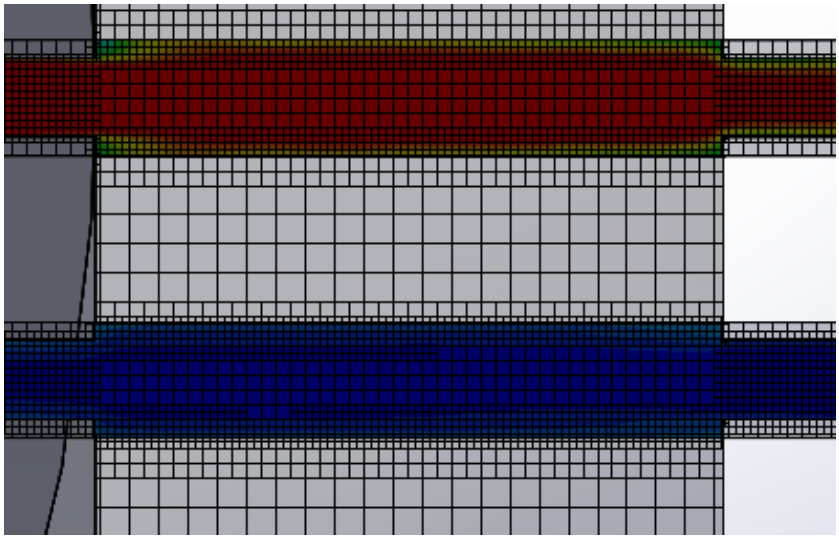

Fig. 19 Run 2 mesh in the area of the outlet tube and lower inlet tube where they pass through the vacuum chamber wall

Looking carefully at Fig. 19, one can see a sharp corner where the tubes terminate in the opening of the hole in the vacuum chamber wall. Figure 20 shows the geometry without the mesh. This step is not an important part of the analysis and should be eliminated in the geometry in the future to ensure a smoother mesh and fewer cells.

Fig. 20 Geometry of the outlet tube and lower inlet tube where they pass through the vacuum chamber wall

Ideally, the mesh should have a minimum of 4 cells through the thickness of critical components where a temperature gradient is expected. Since the tubes are critical and their inner diameter was 0.08 inch and the wall of the tube was 0.02 inch, the ideal gap size for the mesh in this region was 0.005 inch. Runs with the gap size set to 0.005 inch caused the program to crash. The Run and Results sections (Sections 6 and 7) discuss the second run only (minimum gap size = 0.01 inch and level of initial mesh = 5). A comparison of the results of the 2 runs is shown in the Conclusion (Section 8). A discussion of future mesh refinement is provided in Section 9, Future Improvements.

6. Run

Figure 21 provides details on the run time and the number of fluid and solid cells.

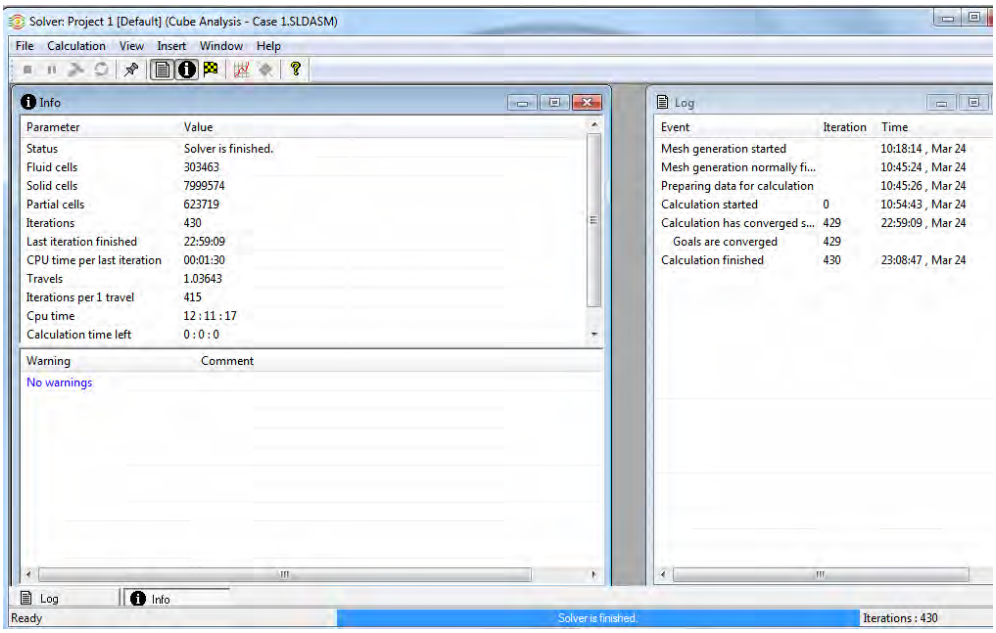

Fig. 21 Run details

7. Results

All of the cross sectional views in the following results are cross sections of the system shown in Fig. 22.

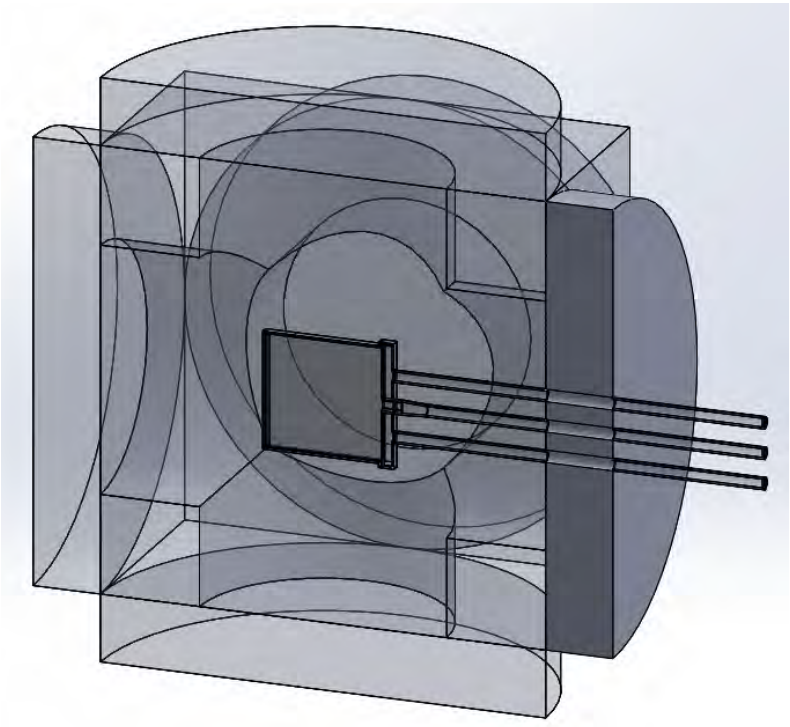

Fig. 22 Cross section of the system

Figure 23 shows the temperature of the solid for the cross section of the system.

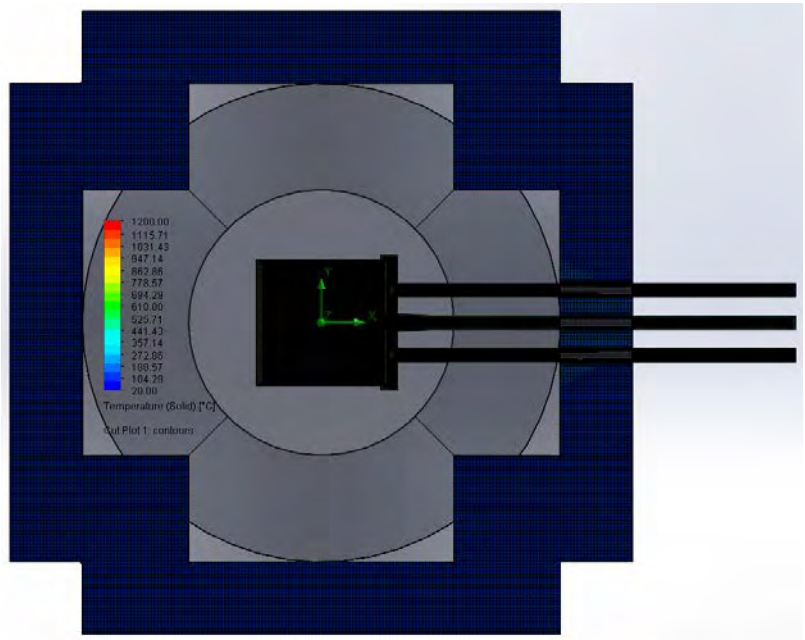

Fig. 23 Temperature of the solids for a cross section of the system

Figures 24, 25, and 26 show close ups of portions of Fig. 23. Note the maximum temperature of the solids in Fig. 24 is approximately 1031 to 1115 °C, as shown by the orange/reddish orange sections. The left end of the combustor is slightly cooler, probably due to the air flow impinging on the inside end of the combustor.

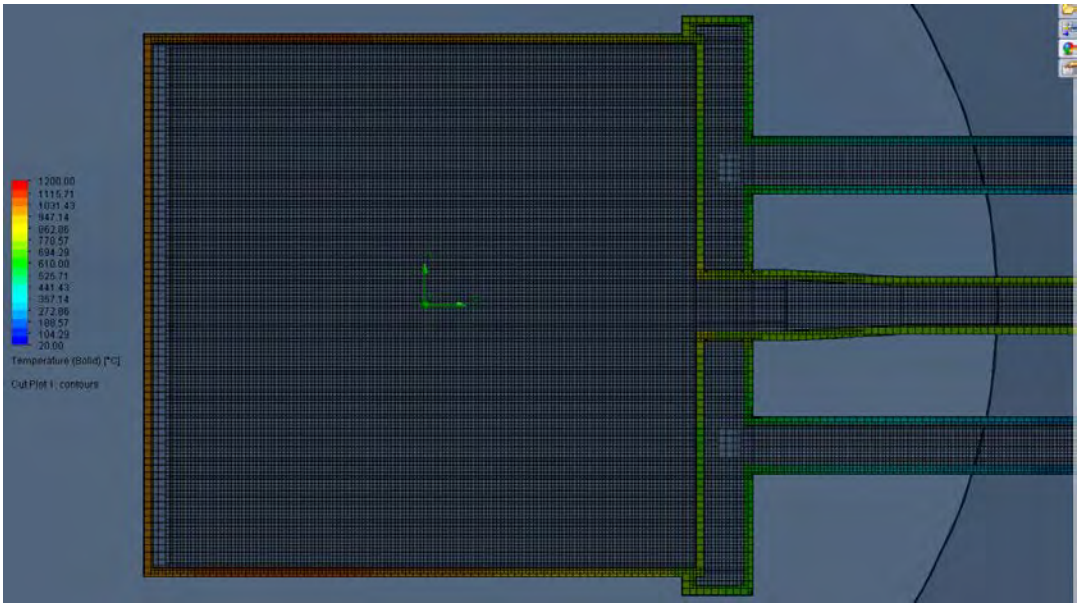

Fig. 24 Temperature of the solids for a cross section of the combustor

Figure 25 shows a close up of the temperature of the outlet tube, lower inlet tube, and vacuum chamber wall. Notice the outlet tube, which is carrying the exhaust from the combustion, is warmer than the inlet tube. This makes sense since the inlet air is at 20 °C.

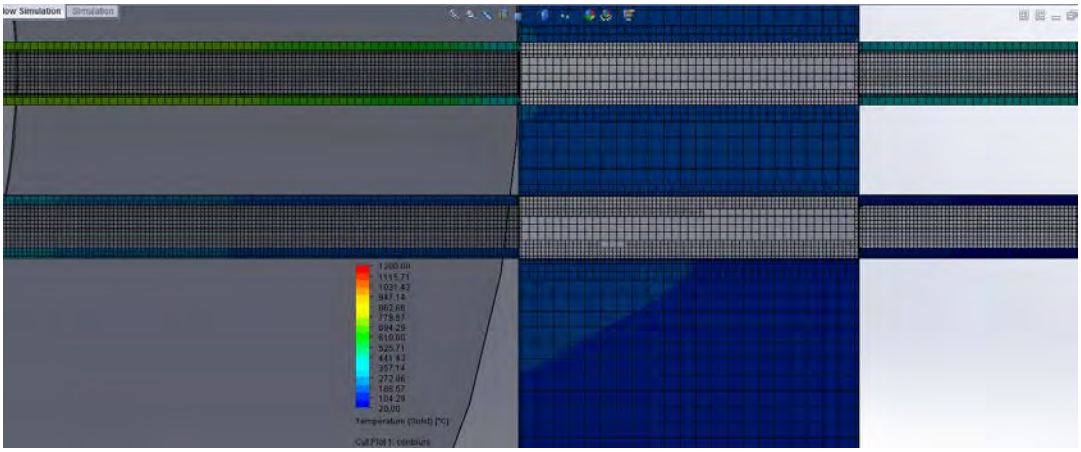

Fig. 25 Temperature of the solids for a cross section of the outlet tube, lower inlet tube, and vacuum chamber wall

Figure 26 shows the close up of the Fig. 25 focusing on the area of the vacuum chamber wall near the outlet and lower inlet tube but with a different color scale to make the temperature differences easier to see. One of the big drivers for the analysis is to determine the temperature of the outer surface of the vacuum chamber wall, inlet tube, and outlet tube. From the figure, it appears the outer surface is at worst approximately 227 to 268 °C. The portion of the inlet tube outside the chamber is approximately 20 to 61 °C. The portion of the outlet tube outside the vacuum chamber near the wall is approximately 268 to 350 °C. The surface of the outlet tube outside the vacuum chamber further away from the wall is approximately 392 to 434 °C. This makes sense since the wall acts as a heat sink helping to cool the outlet tube.

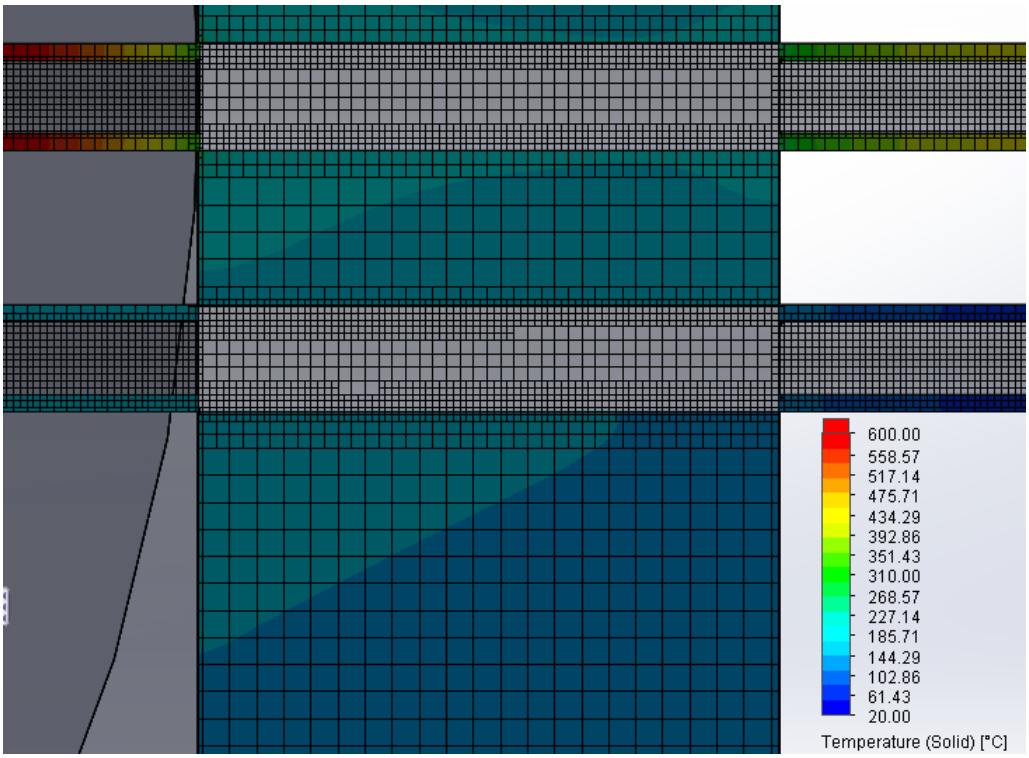

Fig. 26 Temperature of the vacuum chamber wall (note the different color scale)

Figure 27 shows the temperature of the fluid for the cross section of the combustor. As shown by the red area, the fluid in the center of the combustor is approximately 1069 to 1150 °C. Note the fluid temperature is cooler closer to the walls, probably due to heat sinking into the walls. This also holds true for the exhaust leaving the outlet tube and the air entering the inlet tube. For the outlet tube, the temperature of the fluid near the inner wall is approximately 827 to 907 °C, while the fluid near the center of the tube ranges from approximately 907 to 1069 °C. For the inlet tube, the temperature of the fluid near the inner wall is approximately 20 to 100 °C and 342 to 504 °C near the center of the tube.

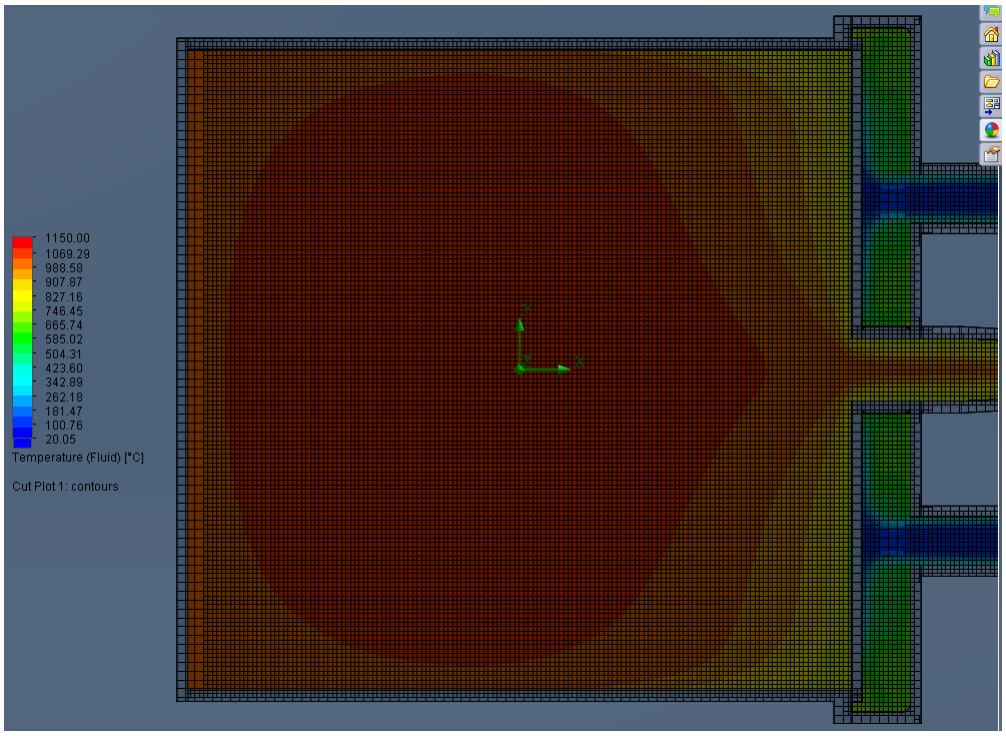

Fig. 27 Temperature of the fluid for the cross section of the combustor

Figure 28 shows the temperature of the fluid in the outlet tube and lower inlet tube from where they attach to the combustor to just outside the vacuum chamber wall.

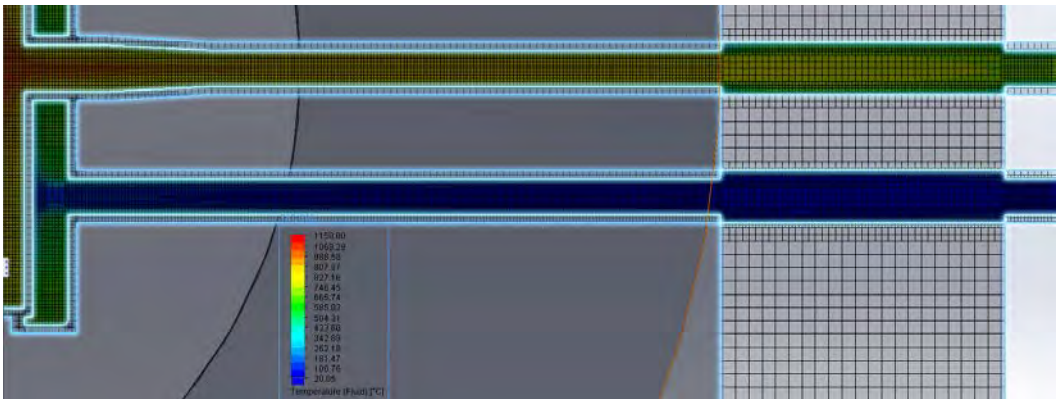

Fig. 28 Fluid temperature in the outlet tube and lower inlet tube

Figure 29 shows the temperature of the fluid in the tube near the vacuum chamber wall and to the opening of the tubes outside the vacuum chamber. Note the change in the temperature scale. Once the fluid is away from the vacuum chamber wall, the temperature profile of the fluid is consistent inside both the inlet and outlet tube. The fluid temperature in the center of the outlet tube appears to be approximately 651 °C, while the temperature near the wall is approximately 457 °C. The fluid temperature in the inlet tube appears to be approximately 20 to 68 °C.

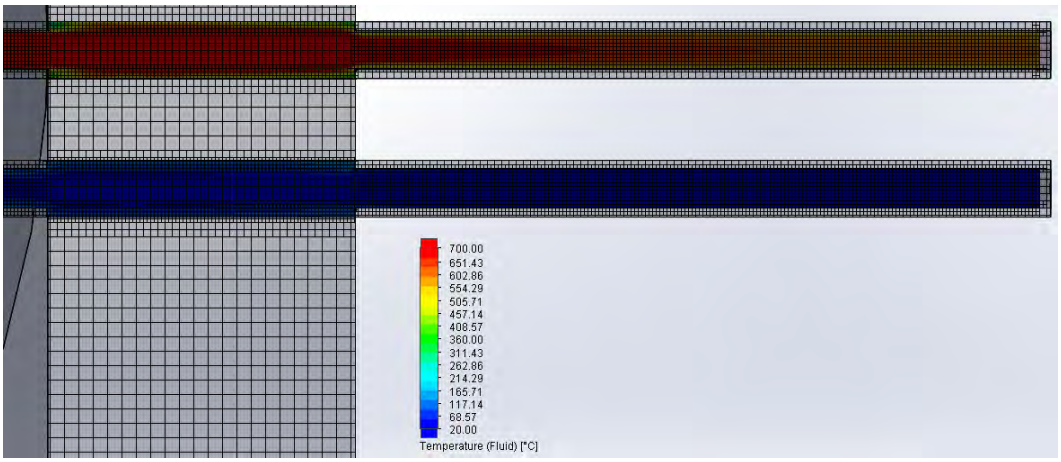

Fig. 29 Fluid temperature in the tube near the vacuum chamber wall and to the opening of the tubes outside the vacuum chamber

Figure 30 shows the temperature of the exterior of the vacuum flange exposed to the large side of the combustor. This flange will be replaced by a viewport, which has a lower operating temperature than the stainless steel flange. The figure shows the maximum temperature is approximately 112 °C.

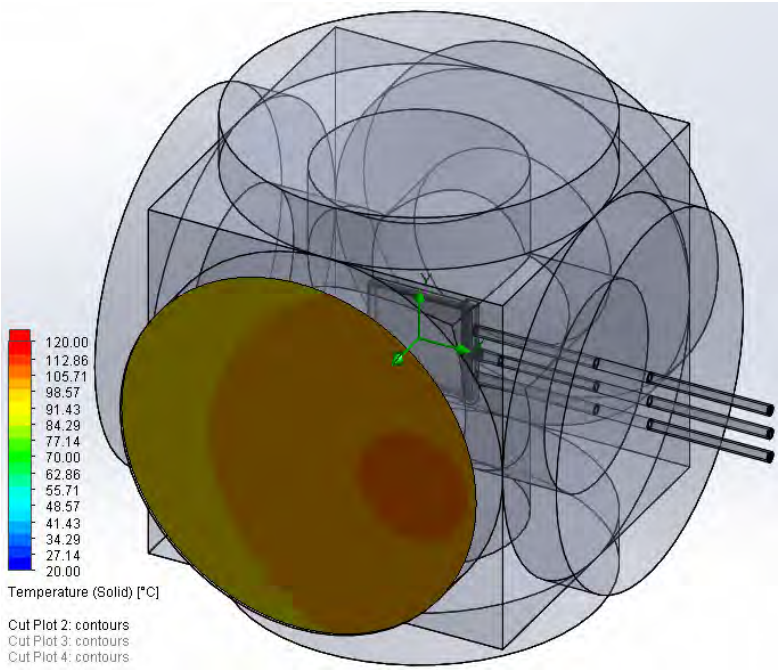

Fig. 30 Temperature of the vacuum flange exposed to the large side of the combustor

Figure 31 shows the temperature of the vacuum chamber surface. The worst-case temperature is approximately 112 °C.

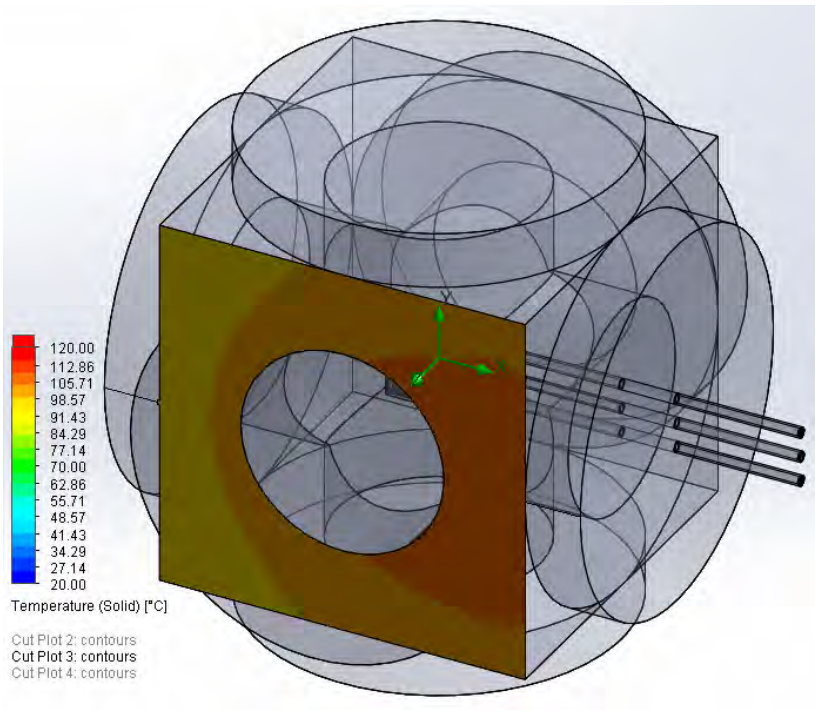

Fig. 31 Temperature of the vacuum chamber surface

Figure 32 shows the temperature of the flange looking at the small side of the combustor. From this figure, the approximate maximum temperature is 103 °C. This is the flange where the mitered elbow with the turbo molecular drag pump will attach.

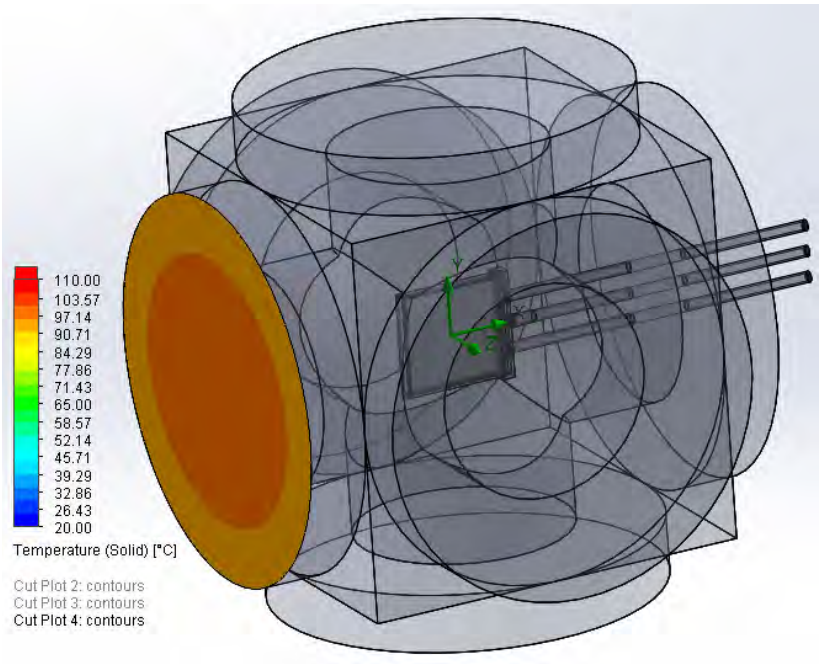

Fig. 32 Temperature of the flange looking at the small side of the combustor

8. Conclusion

The purpose of this report is to estimate the temperatures of various components of the Combustor Test Setup to ensure proper function. Table 1 shows the results of Runs 1 and 2. There are some appreciable differences in certain areas. The temperature of the outer surface near where the tubes attach was cooler for Run 1 than for Run 2, but the temperature of the outlet tube near and far outside the vacuum chamber for Run 1 was hotter than Run 2. It appears the heat-sinking effect of the vacuum chamber wall was not accounted for as well in Run 1 compared to Run 2. The differences in meshing in that area might account for these difference. The issue is discussed in the Mesh section (Section 5).

Table 1 Results of Runs 1 and 2

Location	Run 1 (min gap 0.04 inch and level of mesh = 3) °C	Run 2 (min gap 0.01 inch and level of mesh = 5) °C
Combustor wall	1100	1031–1115
Outer surface of the vacuum chamber near where the tubes attach	144	227–268
Inlet tube near the vacuum chamber wall	20	20–61
Outlet tube near the vacuum chamber wall	632	268 - 350
Outlet tube far outside the vacuum chamber	554	392–434
Fluid in the center of the combustor	1100	1069–1150
Exhaust gas	632	651
Flange where the viewport will be located	120	112
Vacuum chamber surface where the viewport will be located	114	112
Flange where the mitered elbow connected to the pump will be attached	103	103

A more thorough analysis of the effects of the mesh on the results is recommended, but the analysis presented here gives a rough idea of the temperature in critical areas. These critical areas include the temperature of the combustor wall, vacuum chamber wall near the tubes, tubes, exhaust gas, and flanges where the viewport and pump are to be attached. The temperature of the combustor wall is estimated to be 1031–1115 °C, which is at the upper limit of where various properties of the Inconel 600 are measured.[4] As a result, the temperature of the combustor should be monitored carefully. The vacuum chamber wall near the tubes is predicted to reach 227–268 °C, which is well within the operating temperature of Inconel 600.[4]

From a human touch temperature limit, it is good to know that only a small portion of the vacuum chamber is likely to get to this high temperature, although the entire vacuum chamber is predicted to be beyond the heat pain threshold of 43–44 °C[6] when the combustor is running. For the flange where the viewport will be located, the temperature is estimated to reach 112 °C, which is well below the 450 °C maximum operating temperature of the viewport.[7] The most difficult issue for protecting the viewport will be raising the temperature slowly to stay within the 25 °C per minute guideline provided by the manufacturer.[8] Lastly, the temperature of the flange where the elbow leading to the turbo molecular drag pump attaches is estimated to reach 103 °C. This is less than the 120 °C maximum bakeout temperature at the inlet for a CF flange version of the pump selected for the Combustor Test Setup.[9] Also, the elbow will provide additional heat dissipation not accounted for in the analysis thus further reducing the temperature.

9. Future Improvements

As mentioned in the Mesh section (Section 5), the sharp corner where the tubes terminate in the hole in the vacuum chamber wall should be eliminated in the geometry to ensure a smoother mesh and fewer cells.

For the current approach, the analysis can be improved by using symmetry to reduce the number of cells to speed up the calculation. Alternatively, using symmetry allows more cells in critical areas and a smaller minimum gap size to improve accuracy without crashing the program. In addition, the geometry can be simplified further by eliminating discontinuities, such as where the tube and flange connect. This will improve the mesh and require fewer cells. Also, the model could be better matched to the real system by including a simplified elbow and a simplified window with appropriate material properties. The accuracy of the temperature of the combustor needs to be improved. Rather than applying the heat generation rate of 300 W to the entire combustor, if possible, it should be applied to the inside surface of the combustor to better mimic the heat produced by the combustion of the fuel. Lastly, the inlet air needs to be set to a minimum temperature of 150 °C since the incoming fuel and air mixture will be preheated to ensure it is in the vapor state prior to entering the system.

Since we are more concerned with the temperature of the vacuum chamber and components attached to the outside of the vacuum chamber, an alternative analysis might be to assume the combustor surface temperature of 1100 °C (worst case) and inlet flow temperature to the combustor of 300 °C (worst case). This is higher than the planned 150 °C preheat to ensure worse-case conditions.

Another alternative analysis is to assume no flow conditions, but set the combustor surface temperature to 1100 °C (worst case), inlet tubes temperature to 300 °C, and outlet tube to 1100 °C (worst case). This would eliminate modeling the flow in the combustor and show how much heat is conducted from the tubes, and the effects of the radiation on the vacuum chamber and vacuum components. Also, this approach simplifies the mesh by reducing the small volumes inside the tubes that need to be simulated.

10. References

1. Waits MC. Thermophotovoltaic energy conversion for personal power sources. Adelphi (MD): US Army Research Laboratory (US); 2012 Feb. Report No.: ARL-TR-5942.

2. Thermal Fluid Analysis, 2015. Solid Works [accessed 2015]. http://www.solidworks.com/sw/products/simulation/thermal-fluid-analysis.htm.

3. AK Steel Corporation, 304/304L Stainless Steel Product Data Bulletin, Revision 04.25.13 [accessed 2015]. http://www.aksteel.com/markets_products/stainless_austenitic.aspx.

4. Inconel alloy 600, Publication Number SMC-027, Special Metals Corporation, 2008 Sept.

5. Roger CR, Yen SH, Ramanathan KG. Temperature variation of total hemispherical emissivity of stainless steel AISI 304. (Received 29 January 1979), J. Opt. Soc. Am. October 1979;69(10):1387.

6. Ungar E, Stroud K. A new approach to defining human touch temperature standards. Houston (TX): NASA/Johnson Space Center Houston; 2009 Jan. Report No. JSC-CN-19209.

7. Sapphire Del-Seal CF, 2014. MDC Vacuum Products [accessed 2015]. http://www.mdcvacuum.com/DisplayProductContent.aspx?d=MDC&p=i.7.1.2.1.

8. Sapphire single crystal, 2014. MDC Vacuum Products [accessed 2015]. http://www.mdcvacuum.com/DisplayContentPage.aspx?cc=d60c2d6a-4233-407c-8538-ac7de62366b9.

9. New Agilent TwisTorr 84 FS Data Sheet. © Agilent Technologies, Inc. March 2015. Italy.

1 (PDF)	DEFENSE TECH INFO CTR DTIC OCA
2 (PDF)	US ARMY RSRCH LAB IMAL HRA MAIL & RECORDS MGMT RDRL CIO LL TECHL LIB
1 (PDF)	GOVT PRNTG OFC A MALHOTRA
3 (PDF)	US ARMY RSRCH LAB RDRL SED E B ALLMON CM WAITS E TOLMACHOFF

INTENTIONALLY LEFT BLANK.